Journal of Geodesy (2021) 95:51
https://doi.org/10.1007/s00190-021-01496-7

ORIGINAL ARTICLE

Observable quality assessment of broadband very long baseline interferometry system

Ming H. Xu[1,2,3,4] · **James M. Anderson**[3,5] · **Robert Heinkelmann**[5] · **Susanne Lunz**[5] · **Harald Schuh**[3,5] · **Guangli Wang**[4]

Received: 29 November 2019 / Accepted: 4 March 2021 / Published online: 13 April 2021

Abstract
The next-generation, broadband geodetic very long baseline interferometry system, named VGOS, is developing its global network, and VGOS networks with a small size of 3–7 stations have already made broadband observations from 2017 to 2019. We made quality assessments for two kinds of observables in the 21 VGOS sessions currently available: group delay and differential total electron content (δTEC). Our study reveals that the random measurement noise of VGOS group delays is at the level of less than 2 ps (1 ps $= 10^{-12}$ s), while the contributions from systematic error sources, mainly source structure related, are at the level of 20 ps. Due to the significant improvement in measurement noise, source structure effects with relatively small magnitudes that are not overwhelming in the S/X VLBI system, for instance 10 ps, are clearly visible in VGOS observations. Another critical error source in VGOS observations is discrete delay jumps, for instance, a systematic offset of about 310 ps or integer multiples of that. The predominant causative factor is found to be related to source structure. The measurement noise level of δTEC observables is about 0.07 TECU, but the systematic effects are five times larger than that. A strong correlation between group delay and δTEC observables is discovered with a trend of 40 ps/TECU for observations with large structure effects; there is a second trend in the range 60–70 ps/TECU when the measurement noise is dominant.

Keywords VGOS observations · Ionosphere effects · VLBI · IVS · Space geodesy · Radio astronomy

1 Introduction

Geodetic very long baseline interferometry (VLBI) is a space-geodetic technique that has regularly made global astrometric/geodetic observations since 1979, which are the basis for creating the International Celestial Reference Frame (ICRF2; Fey et al. 2015) and obtaining a full set of Earth Orientation Parameters. Together with the other three space geodetic techniques, VLBI plays an important role in establishing the International Terrestrial Reference Frame (ITRF2014; Altamimi et al. 2016). At the beginning of this century, the International VLBI Service for Geodesy and Astrometry (IVS;[1] Schuh and Behrend 2012; Nothnagel et al. 2017) proposed to develop the next-generation geodetic VLBI system, initially called VLBI2010 (Niell et al. 2006) but subsequently renamed the VLBI Global Observing System (VGOS). This new VLBI system relies mainly on the advantages of small (∼ 12 m in diameter) and fast-slewing antennas, ultra-wide observing frequency receivers (from 2 to 14 GHz), and the expectation of continuous operation, 24 h a day and seven days a week (Petrachenko et al. 2009). In order to achieve its goal of 1 mm position accuracy and 0.1 mm/year velocity stability on global scales, the first strategy proposed by the VGOS working group was to reduce the random noise component of the group delays (Niell et al. 2007). Building a global VGOS network with a sufficient

✉ Ming H. Xu
minghui.xu@aalto.fi

1 Aalto University Metsähovi Radio Observatory, Metsähovintie 114, FI-02540 Kylmälä, Finland

2 Aalto University Department of Electronics and Nanoengineering, PL15500, FI-00076 Aalto, Finland

3 Institut für Geodäsie und Geoinformationstechnik, Fakultät VI, Technische Universität Berlin, Sekr. KAI 2-2, Kaiserin-Augusta-Allee 104-106, 10553 Berlin, Germany

4 Shanghai Astronomical Observatory, Chinese Academy of Sciences, Shanghai 200030, China

5 GFZ German Research Centre for Geosciences, Helmholtz Centre Potsdam, Telegrafenberg 14473, Potsdam, Germany

[1] https://ivscc.gsfc.nasa.gov/index.html.

number of stations is in progress, and a small VGOS network has started to make broadband observations. The technical implementation of the VGOS system can be found in Niell et al. (2018), and the data correlation and processing of VGOS observations from a single baseline can be referred to in Kondo and Takefuji (2016) and Niell et al. (2018). Analyzing these actual VGOS observations allows us to investigate the measurement noise level and the systematic behaviors of the VGOS observations.

In this paper we investigate the contribution of random measurement noise and systematic error sources in VGOS delay and differential total electron content (δTEC) observables.[2] The relationship between these two types of observables is also studied. We use a different method of assessing the error level of the VGOS system than that in Elosegui et al. (2018) and Niell et al. (2018), who demonstrated the post-fit residuals from geodetic VLBI solutions. Furthermore, instead of studying observations of one short baseline, we present the results of VGOS observations from a global network. In Sect. 2 we present the VGOS observations currently available and introduce the method of data analysis that we used. A quality assessment of group delay observables is given in Sect. 3. In Sect. 4 we demonstrate the measurement noise level and systematic errors in δTEC observables, estimated simultaneously in VGOS observations. The strong correlation between VGOS group delay and δTEC observables is studied in Sect. 5. In Sect. 6, we summarize and discuss the results.

2 Broadband VLBI observations and data analysis

The IVS conducted a continuous observing campaign with three VLBI networks (two legacy S/X networks and one VGOS broadband network) in 2017, called CONT17 (Behrend et al. 2020). The VGOS broadband network in CONT17 had a smaller number of stations than the two legacy networks, and it observed only for one third of the whole CONT17 period. However, it provides the first public data set of the VGOS broadband system, which was originally proposed about 20 years ago. As of 15 November 2019, 16 other VGOS sessions carried out in 2019 were released,[3] as listed in Table 1. On average, 24-h VGOS sessions obtain about 2.2 times as many as scans[4] than the legacy 24-h VLBI sessions. These broadband observations were made simultaneously at four 512-MHz-wide bands centered at 3.2, 5.5, 6.6 and 10.4 GHz. (The detailed technical description of the observing frequency setup is available in Niell et al. (2018).) The median and mean of the formal errors for group delay and δTEC observables in each session are also shown in the table. The median formal errors of group delay observables for these 21 sessions are in the range of 1.2 ps (1 ps = 10^{-12} s) to 3.0 ps, and those for δTEC observables are in the range of 0.029 TECU (1 TECU = 10^{16} electrons per square meter) to 0.060 TECU.

We processed the 21 VGOS sessions to determine error contributions in group delay observables, including measurement noise and source structure effects, by doing closure analysis (Xu et al. 2016, 2017; Anderson and Xu 2018). We adopted the same procedure of closure analysis for the VGOS sessions as was developed for the CONT14 sessions described in Anderson and Xu (2018). (The technical description of our closure analysis can be found in the supplemental information to Anderson and Xu (2018).) In short, the method of closure analysis statistically determines the baseline equivalent delay error of each individual observation[5] from all the available closure delays involving that observation, called closure-based error estimate; the weighted root-mean-square (WRMS) delay error of a group of data can then be derived by combining the closure-based error estimates of the delay observables in the group. The method has two major advantages: (1) the station-based errors[6] are canceled out exactly in closure delays; and (2) complementary to the post-fit residuals from geodetic solutions, it provides an independent way of assessing the observable quality. Except for baseline clocks, which in some cases are included in the parameterization as a constant offset in delays for a specific baseline and can thus only reduce a constant offset in closure delays, no geodetic parameters in a routine VLBI solution can absorb nonzero closure delays. They therefore contribute entirely to the residuals of the VLBI solution and can bias the estimates of geodetic parameters. In the recent research of Bolotin et al. (2019), structure model parameters were included in the VLBI solution of the CONT17 VGOS sessions to reduce the large residual delays of the sources 0552

[2] An observable refers to a specific kind of quantity, such as amplitude, phase, delay or rate, that has been measured by maximizing the correlation between the recorded signals of a distant radio source at the two stations of a baseline; in addition, δTEC estimate is included as another kind of observable in VGOS.

[3] Data are available through the NASA CDDIS server: https://cddis.nasa.gov/archive/vlbi/ivsdata/vgosdb/.

[4] A scan consists of simultaneous observations of a radio source by two or more stations over an interval on the order of 5 s to 2 min.

[5] In the remainder of this paper, "observation" is used with the restricted meaning of a pair of two stations—a baseline—observing a radio source over a short duration, typically on the order of 5 s to 2 min.

[6] We refer to effects such as atmosphere, ionosphere, clock, and geometry as station-based—when there is a change at one epoch for a station for any of these effects the corresponding changes with the same magnitude will happen to all the observations on the baselines of that station within the scan of that epoch—and the errors in modeling these effects as station-based errors.

Table 1 Observing sessions of the VGOS broadband network

Date (yyyy/mm/dd) (1)	Session name (2)	Number of scans (3)	Number of observations (4)	Number of sources (5)	Station list (6)	Delay formal err. Median (ps)	Delay formal err. Mean (ps)	δTEC formal err. Median (TECU)	δTEC formal err. Mean (TECU)
2017/12/03	B17337	1180	5999	67	GsIsK2YjWfWs	1.71	2.12	0.039	0.046
2017/12/04	B17338	1170	5037	66	GsIsK2YjWfWs	3.01	5.00	0.060	0.098
2017/12/05	B17339	1180	5833	65	GsIsK2YjWfWs	2.86	4.86	0.057	0.095
2017/12/06	B17340	1130	5166	66	GsIsK2YjWfWs	2.41	4.50	0.051	0.089
2017/12/07	B17341	1246	6043	66	GsIsK2YjWfWs	2.43	4.47	0.050	0.088
2019/01/07	VT9007	1132	8310	64	GsK2OeOwYjWfWs	1.70	2.37	0.039	0.049
2019/01/22	VT9022	1024	6070	64	K2OeOwYjWfWs	1.45	2.00	0.035	0.043
2019/02/04	VT9035	1043	4622	64	GsK2OeYjWfWs	1.39	1.72	0.036	0.042
2019/02/19	VT9050	1115	7668	62	GsK2OeYjWfWs	1.37	1.79	0.035	0.042
2019/03/04	VT9063	1129	7645	63	GsK2OeYjWfWs	1.34	1.76	0.033	0.041
2019/03/18	VT9077	1080	5586	61	GsK2OeYjWfWs	1.29	1.77	0.032	0.041
2019/04/01	VT9091	1121	7651	62	GsK2OeYjWfWs	1.43	1.83	0.034	0.042
2019/04/15	VT9105	1105	5102	61	GsK2OeWfWs	1.44	1.85	0.035	0.043
2019/04/29	VT9119	1126	5142	63	GsK2OeWfWs	1.72	2.19	0.040	0.048
2019/05/13	VT9133	1123	4120	63	GsK2OeWfWs	1.71	2.25	0.038	0.048
2019/05/28	VT9148	676	1444	60	GsOeWs	1.21	1.67	0.031	0.039
2019/06/11	VT9162	1125	4891	64	GsK2OeWfWs	1.43	1.84	0.034	0.041
2019/06/24	VT9175	1110	5097	66	GsK2OeWfWs	1.71	2.20	0.039	0.047
2019/07/08	VT9189	776	1860	60	GsOeWs	1.17	1.64	0.029	0.037
2019/07/22	VT9203	1093	6235	67	GsK2OeOwWfWs	1.94	2.44	0.042	0.050
2019/08/05	VT9217	1174	11541	74	GsK2OeOwYjWfWs	1.63	2.29	0.039	0.050

Two-letter station codes in column 6 have the following meanings: Gs=GGAO12M, Is=ISHIOKA, K2=KOKEE12M, Yj=REAGYEB, Wf=WESTFORD, Ws=WETTZ13S, Oe=ONSA12NE, and Ow=ONSA12SW. Refer to ftp://cddis.gsfc.nasa.gov/pub/vlbi/ivscontrol/ns-codes.txt for more information about these stations. The values in the last four columns are the median and mean of the formal errors for group delay and for the δTEC observables for observations with SNR > 7

$+ 398$ and $2229 + 695$, which can thus reduce the magnitudes of the delay misclosures. However, the method has not been demonstrated to be applicable to general cases of radio sources with structure at different scales or insufficient numbers of observations. In the paper, closure delays, measuring intrinsic structure of sources as closure phases and closure amplitudes, are treated as errors in VGOS broadband delays only because the effects of source structure bias the geodetic parameters.

Closure analysis was also applied to the estimated ionosphere-like phase dispersion parameter, called δTEC, from these VGOS sessions. δTEC is the difference of the total electron content (TEC) along the line of sight from a source to each station of a baseline during a scan. Closure δTEC over a triangle of three antennas therefore gives insight into the errors in δTEC measurements.

The conditions for the exclusion of an observation, called flagging, are summarized here: (1) observations with signal-to-noise ratio (SNR) less than 7; (2) station RAEGYEB from the second day to the last day of CONT17 VGOS observations, that is the sessions B17338, B17339, B17340 and B17341; and (3) all the observations on the baseline ONSA13NE–ONSA13SW.

For completeness, we briefly recall the basic equations of the closure analysis and describe the terminology used. Closure delay is the sum of delay observables over a closed triangle of three stations. For a triangle of three stations, a, b, and c, closure delay is defined by

$$\tau_{\mathrm{clr}} \equiv \tau_{ab} + \tau_{bc} + \tau_{ca}, \tag{1}$$

where, for instance, τ_{ab} is the delay observable from station a to station b. The reference-time convention in geodetic VLBI defines that the timestamp of the delay observable as the time of arrival of the wavefront at the first antenna of a baseline. For instance, delay $\tau_{ab}(t_0)$ refers to the delay for a wavefront that arrives at station a at epoch of t_0. Therefore, the geodetic delay observables for multiple baselines in a scan, although they have the same timestamp, do not necessarily refer to the same wavefront. When these delay observables are used to derive closure delays, a correction is needed to make the geometry of a triangle completely close; detailed

discussions and dedicated equations can be found in Section 2 of Xu et al. (2016) and in Section 4.1 of Anderson and Xu (2018). An alternative way of forming closure delays is to use the delay observables with geocentric timestamps (the astronomical convention), rather than the delay observables used in geodetic solutions; the former need no correction.

The uncertainty of a closure delay is calculated from the formal errors of the three observables forming it by assuming that they are independent.

For the delay observable τ_{ab} at a single epoch, its closure-based error estimate, $\Delta\tau_{ab}$, is statistically determined from all the closure delays that are formed by τ_{ab} together with the other un-flagged observations in the scan at that epoch, written as

$$\Delta\tau_{ab} = \frac{\sum_{i=1}^{N} |\tau^{i}_{\mathrm{clr}-ab}|}{\sqrt{3}N}, \tag{2}$$

where N is the number of such closure delays and $\tau^{i}_{\mathrm{clr}-ab}$ is the ith one. The number $\sqrt{3}$ in the denominator scales the mean closure delay to derive a baseline equivalent error by assuming that the errors in different observations are independent. This process as defined by Eq. 2 for the observable τ_{ab} was repeated for all observations one by one to derive their closure-based error estimates, $\Delta\tau$, whenever possible.

The WRMS delay error (not uncertainty), $\delta\tau$, is obtained by combining the closure-based error estimates as follows:

$$\delta\tau = \sqrt{\frac{\sum_{j=1}^{l} w_j (\Delta\tau^j)^2}{\sum_{j=1}^{l} w_j}}, \tag{3}$$

where l is the number of un-flagged observations with closure-based error estimates available in a data group of interest (e.g., all observations of a particular source or some selected sources or all observations in one session), $\Delta\tau^j$ is the closure-based error estimate of the jth observation, and w_j is its weight. The weighting is done by setting an equal weight for all the delay observables, named uniform weighting, or by using the reciprocal of the square of the uncertainty (formal error) of each individual delay, named natural weighting. (The uniform and natural weighting schemes used here have different meanings to those used in the astrophysical imaging studies.) The same procedure of this closure analysis was applied to study δTEC measurements; closure δTEC, closure-based error estimate of δTEC and WRMS δTEC error are likewise defined.

Note that the closure analysis derives the *baseline equivalent* error for each observation from closure quantities. It is obvious that the closure-based error estimate of an observation is affected (can be enlarged or reduced) by source structure effects and measurement noise in the observations of the other baselines in the scan. It is not appropriate to use closure-based error estimate to quantify the errors at the level of a single observation; however, the aim of closure analysis is to use closure-based error estimates only to determine the overall variance of source structure effects and measurement noise for a given group of data, as defined by Eq. 3. In this case, it will work without introducing significant biases when the random measurement noise, independent between different observations, is the dominant error source. On the other hand, if the systematic error sources dominate, the mean of the absolute values of all the closures formed with a common observation maximizes the possibility of determining these systematic errors in that observation; it was then scaled by a factor of $\sqrt{3}$ to reduce the contributions of systematic errors in the other observations forming those closures. Nevertheless, in the presence of systematic errors, the assumption for Eq. 2 is not satisfied. It can lead to biases in interpreting the derived WRMS delay errors as the magnitudes of source structure effects that one would expect to have in the post-fit residuals from geodetic solutions. In order to investigate the potential biases, the median was used in place of the mean in Eq. 2 as an alternative statistic to derive closure-based error estimates and the corresponding WRMS errors.

In closure analysis, we also directly compare the closure delays for a given source between various triangles and for a specific triangle between different sources, which can yield insight into the properties of individual sources, baselines, and stations.

3 Group delay observables

3.1 Measurement noise

A closure-based delay error estimate could be derived for 88% of the observations in the 21 VGOS sessions, while 5% did not form any closure with un-flagged observations, and 7% were flagged as described in the previous section. Based on the uniform weighting and the natural weighting schemes, the WRMS delay error was calculated from these closure-based error estimates for each individual session and for all 21 sessions combined. The results are shown in Table 2.

Apart from session VT9007, the WRMS delay errors for the other 20 sessions are in the range of 18.5–26.8 ps based on the uniform weighting and in the range of 14.1–28.5 ps based on the natural weighting. The WRMS delay errors for the 21 sessions combined, labelled as "ALL" in the table, are about 23 ps and 21 ps based on the two weighting schemes. This is a significant improvement compared to the corresponding values of 35.3 ps (uniform) and 25.2 ps (natural) for the CONT14 sessions(Anderson and Xu 2018), which represent the best observing campaign of the legacy S/X VLBI system.

For session VT9007 the WRMS delay errors are remarkably high—36 ps and 34 ps from the two weighting schemes.

Table 2 WRMS delay errors determined by closure analysis (in units of picoseconds)

Session/group (1)	N_{obs} (2)	N_{CloErr} (3)	Uniform weighting (4)	Natural weighting (5)
B17337	5999	5620	22.5	17.9
B17338	5037	3279	26.8	19.1
B17339	5833	3556	20.6	17.2
B17340	5166	3042	24.4	20.3
B17341	6043	3742	24.1	21.1
VT9007	8310	7508	36.1	33.8
VT9022	6070	5222	23.3	18.9
VT9035	4622	4283	18.5	14.1
VT9050	7668	7511	18.8	17.0
VT9063	7645	7503	20.9	19.3
VT9077	5586	5294	20.7	17.4
VT9091	7651	7325	21.0	21.1
VT9105	5102	4835	19.2	18.6
VT9119	5142	4856	21.0	25.4
VT9133	4120	3786	21.7	17.7
VT9148	1444	1146	22.9	25.4
VT9162	4891	4583	21.5	19.2
VT9175	5097	4830	21.3	16.9
VT9189	1860	1611	23.6	28.5
VT9203	6235	5827	20.9	26.0
VT9217	11,541	11,348	22.7	20.6
ALL	121,062	106,707	22.9	21.0
ALL-19	106,682	93,977	21.5	20.0
CARMS-0.25	20,998	17,702	6.2	2.4

N_{obs} is the number of observations in each session or subgroup of data, and N_{CloErr} is the number of observations that were not flagged out and formed at least one closure delay with un-flagged observations allowing the derivation of closure-based error estimates

This is due to an exceptionally large number of misclosures of about 310 ps or −310 ps in the closure delays, as shown in Fig. 1. The vast majority of these misclosures involve station ONSA13SW, due to its phasecal problem at the 6.6-GHz frequency band (Brian Corey, personal communication, September 7, 2020). After 390 closure delays of station ONSA13SW with absolute values of about 310 ps were flagged, the WRMS delay error for session VT9007 was redetermined to be 23.0 ps (uniform) and 18.9 ps (natural). The WRMS delay errors for the "ALL" group were recalculated from the 19 sessions excluding VT9007 and VT9022—the latter session undergoes the same issue but with offsets of around 1100 ps and −1100 ps, also related to station ONSA13SW, but not as many. The WRMS delay errors for the 19 sessions are 21.5 ps (uniform) and 20.0 ps (natural), labelled as "ALL-19" group in Table 2. In summary, we argue that the magnitude of the random measurement noise and the systematic errors in the VGOS observations is in the range of 20.0–22.9 ps.

Except for sessions like VT9148 and VT9189 with an observing network of three stations, the natural weighting scheme generally gives significantly smaller values of the WRMS delay error than the uniform weighting scheme. This is to be expected when the non-Gaussian delay values due to source structure are added to the closure delays with an otherwise noise-like distribution. On the other hand, because source structure effects not only cause structure delays in delay observables but also reduce observed amplitudes and thus the observations' SNR, natural weighting will underestimate the magnitude of their actual impacts. Thus, while the natural weighting statistics are appropriate for evaluating the properties of the delay/δTEC observables, the uniform weighting statistics can be useful for identifying sources with systematic errors, such as those due to source structure. Furthermore, the SNRs of VGOS observations are typically very high, for instance, the median SNR for the CONT17 VGOS observations is ∼90; uniform weighting should be used to investigate the systematic error levels, especially if these systematic errors are significantly larger than the ran-

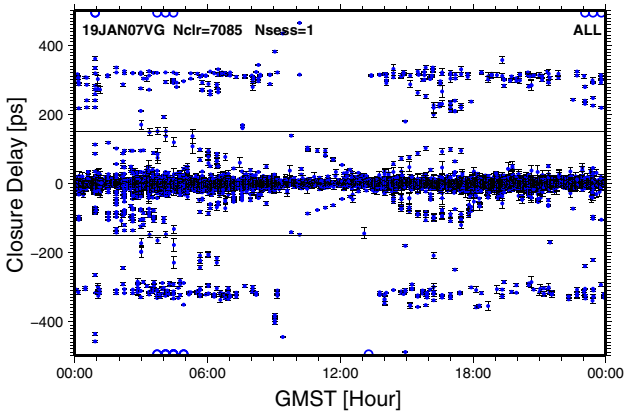

Fig. 1 All closure delays of session VT9007 excluding triangles with baseline ONSA13NE–ONSA13SW. Closure delay uncertainties are shown as black bars. There are 7085 closure delays in total. A large number of closure delays with an absolute offset of about 310 ps is visible. All the closure delays exceeding the limits of the *Y* axis are shown on the top or bottom of the plot as open circles. This convention applies to all of the closure plots in the paper; plots with no open-circle points on the bottom and top have no excessively large closure delays. Two solid horizontal lines with an absolute value of 150 ps are provided as guides

dom measurement noise and are correlated with the SNRs, for example, source structure effects.

In order to further investigate the random measurement noise level in VGOS sessions, we adopted the closure amplitude RMS (CARMS) values based on the basic weighting scheme[7] from Table 2 in Xu et al. (2019) to identify the sources with minimum structure in these VGOS sessions. For the definition of CARMS, please consult equations (2)–(4) and (6)–(8) in Xu et al. (2019). The CARMS value of each individual source was calculated using all the available closure amplitudes for X-band only from historical VLBI observations from 1980 to Aug. 2018 (no VGOS broadband observations are included). Apart from thermal noise, observations of an ideal point source will always give log closure amplitudes[8] equal to zero, while those of radio sources with extended structure will have log closure amplitudes deviating from zero, leading to larger CARMS values. Hence, in general, a smaller CARMS value of a source indicates that it causes less structure effects. Our recent study has demonstrated the correlation between the magnitudes of the radio-to-optical source position differences and CARMS values (Xu et al. 2021b). Using a maximum CARMS limit of 0.25 to select sources with minimum structure, 28 low-structure sources were found in the VGOS measurements, shown in Table 3. The CARMS value of 0.25 was chosen as a compromise in order to have a sample of radio sources with both minimum structure and a sufficient number of observations. These 28 sources are associated with 19.7 percent of the observations in the 19 VGOS sessions (excluding sessions VT9007 and VT9022). The WRMS delay error value for these observations, labelled as "CARMS-0.25" in Table 2, is 6.2 ps for the uniform weighting and only 2.4 ps for the natural weighting. As we explained already, the uniform weighting indicates the systematic error contribution and the natural weighting tends to show the measurement noise level. We therefore conclude that the VGOS measurement noise is no larger than the 2 ps level as demonstrated by

Table 3 Source group with CARMS less than 0.25, CARMS-0.25 for short

IVS Design. (1)	CARMS (2)	N_{obs} (3)	ICRF3 category (4)
0048−097	0.11	95	D
0054+161	0.10	56	D
0133+476	0.23	2906	D
0237−027	0.15	193	D
0446+112	0.24	589	O
0529+483	0.21	3120	D
0536+145	0.17	13	D
0627−199	0.15	92	D
0656+082	0.24	36	O
0716+714	0.20	4865	D
0723+219	0.18	13	O
0727−115	0.24	727	D
0804+499	0.20	211	D
1040+244	0.17	815	D
1124−186	0.21	312	D
1243−160	0.13	288	D
1300+580	0.18	1386	D
1417+385	0.17	53	O
1519−273	0.18	119	D
1636+473	0.24	141	D
1749+096	0.22	1163	D
1908−201	0.20	222	D
2059+034	0.24	33	D
2141+175	0.21	730	O
2215+150	0.22	1656	D
2227−088	0.24	692	D
2255−282	0.18	89	O
2309+454	0.21	383	O

The CARMS values in column 2 are taken from Xu et al. (2019), and the ICRF3 categories in column 4 are from http://hpiers.obspm.fr/icrs-pc/newwww/icrf/icrf3sx.txt. D means defining sources, i.e., this particular source was included for the definition of the reference frame axes, and O means other non-defining sources. N_{obs} in column 3 is the total number of VGOS observations in these 21 sessions for each source

[7] It assumes that the noise floor in log closure amplitudes is 0.1 and thus adds 0.1 to their formal errors in the quadrature sense for weighting.

[8] Note that the natural logarithm was adopted in the definition of closure amplitude to calculate CARMS values, as shown in the equation (3) in Xu et al. (2019).

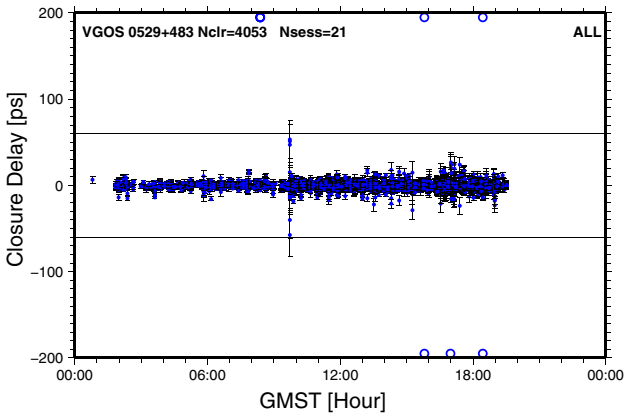

Fig. 2 All closure delays of source 0529+483 in the 21 VGOS sessions with black bars giving the $1-\sigma$ measurement uncertainties based on the formal errors of delay observables. There are four closure delays of about 310 ps from one scan of session VT9007 showing as one open circle on the top right of the figure and five closure delays of about 1100 ps or −1100 ps from three scans of session VT9022 shown on the top and bottom of the figure. The WRMS of all the available closure delays excluding these 9 is only 3.0 ps from natural weighting. Source 0529+483 demonstrates the measurement noise level in VGOS delays, which should obviously be below 3 ps. Two solid horizontal lines with an absolute value of 60 ps are provided as guides

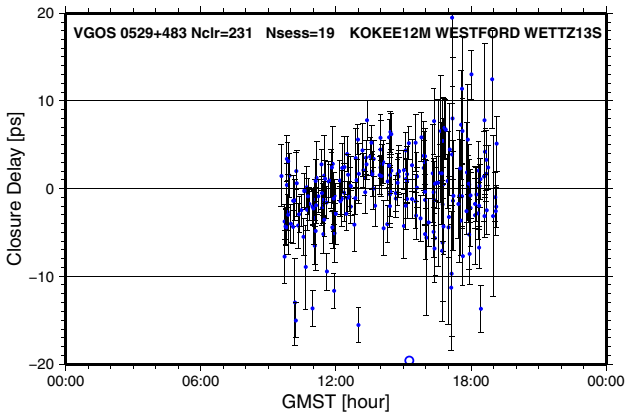

Fig. 3 Zoom-in plot of closure delays of source 0529+483 for triangle KOKEE12M–WESTFORD–WETTZ13S. They are not randomly distributed around zero, suggesting that there are systematic effects with a magnitude of a few picoseconds for this source. Three solid horizontal lines are provided to guide the reader

the sources with minimum structure, and the contributions of systematic errors for these sources are at the level of 5 ps to 6 ps. Taking source 0529+483 as an example, all available closure delays in the 21 sessions are shown in Fig. 2. If the four closure delays in VT9007 with an offset of 310 ps and the five closure delays in VT9022 with offsets of 1100 ps or −1100 ps are excluded, the WRMS closure delay for source 0529+483 is only 3.0 ps. However, its closure delays, when inspecting one specific triangle at scales of a few tens of picoseconds, are still not randomly distributed, as shown in Fig. 3. Even though the magnitude of the systematic variations is only about 10 ps, they are visible in the plot. Similar or even larger systematic variations were detected for other CARMS-0.25 sources, such as 0716+714 and 0133+476.

As discussed at the end of Sect. 2, the median value was also used to derive closure-based error estimates and then to calculate the corresponding WRMS delay errors. The differences in WRMS delay error values between the two techniques are very small for both weighting schemes, no more than 0.5 ps in most cases.

3.2 Source structure effects

As we did for the historical S/X VLBI observations (Xu et al. 2019), it is beneficial to show a few closure plots for several sources with different magnitudes of structure effects as examples to understand those effects in the broadband VLBI system.

0059+581 Closure delay plots for source 0059+581 are shown in Fig. 4 for two triangles, GGAO12M–ISHIOKA–WETTZ13S and KOKEE12M–WESTFORD–WETTZ13S. The first triangle was observed only in CONT17 and has 119 closure delays in total. The pattern of two peaks with opposite signs separated by a 12-h GMST period is a normal behavior of source structure effects. The second triangle, which was observed in 18 VGOS sessions, produced 329 closure delays. Through it, the source-structure time evolution is well demonstrated: the peak in the closure delay pattern changed from −30 ps in Dec. 2017 to around 0 ps in early 2019, increased to +60 ps in March and decreased back to +30 ps in the middle of 2019. Source 0059+581 is a very typical geodetic source and has been the most frequently observed source both by the legacy VLBI system and the VGOS system so far. For the triangle GGAO12M–ISHIOKA–WETTZ13S, it is seen that the structure effects have a magnitude of as large as 20 ps but the WRMS closure delay is only 6.9 ps. Source structure effects are more easily visible in VGOS observations than in the legacy VLBI observations because the measurement noise in VGOS is well below 3 ps. This is one reason why source structure effects are so critical for VGOS.

0016+731 Source 0016+731 is another of the important geodetic sources. The closure delays for source 0016+731 are shown in Fig. 5 for triangle KOKEE12M–WESTFORD–WETTZ13S, which is the same triangle shown in Fig. 3 for source 0529+483 and in the bottom plot of Fig. 4 for source 0059+581. It has 460 closure delays in 19 VGOS sessions. The source structure changed significantly from 2017 to 2019. The magnitudes of structure effects are as large as 100 ps in 2019.

3C418 Source 3C418 is a representative of the extremely extended sources in geodetic VLBI and has been observed

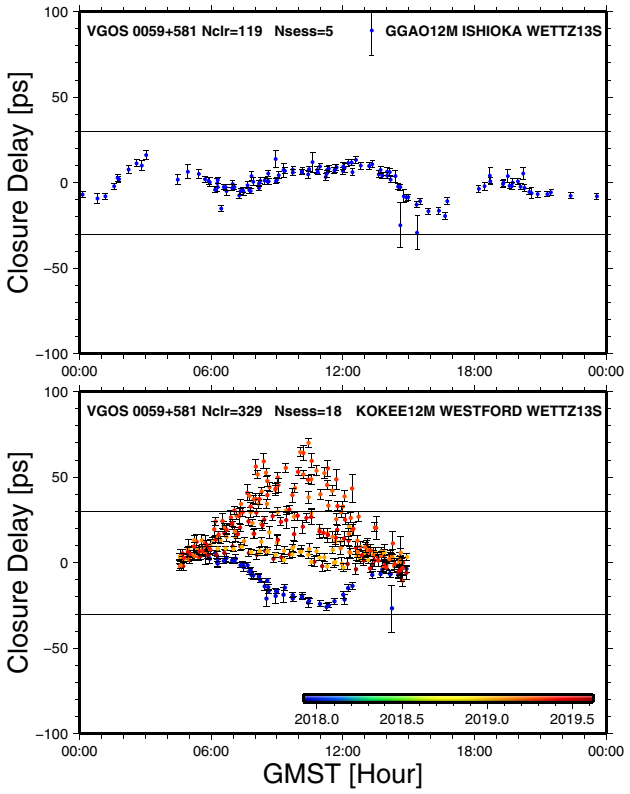

Fig. 4 Closure delays for source 0059+581 as a function of GMST for two triangles, GGAO12M–ISHIOKA–WETTZ13S (top) and KOKEE12M–WESTFORD–WETTZ13S (bottom). The color coding indicates the observation date, and the corresponding legend is shown on the bottom-right corner of the bottom plot. The top plot shows a normal pattern of source structure effects, while the bottom one clearly shows the source-structure time evolution from CONT17 in Dec. 2017 to 2019 and even within 2019. Two solid horizontal lines with an absolute value of 30 ps are provided as guides

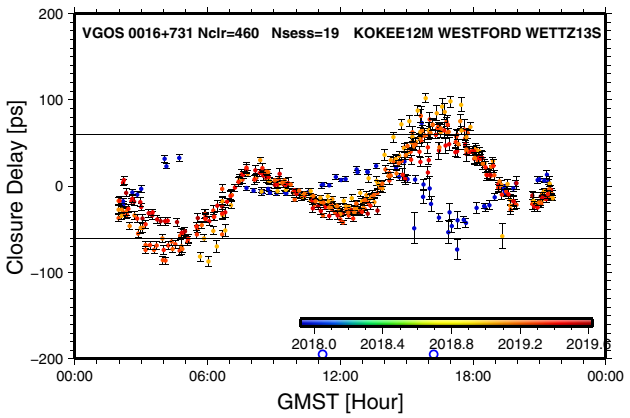

Fig. 5 Plot of closure delays for source 0016+731 as a function of GMST for triangle KOKEE12M–WESTFORD–WETTZ13S, which was shown also for source 0529+483 in Fig. 3 and for source 0059+581 in the bottom of Fig. 4. Source 0016+731 is another one of the important geodetic sources. However, its structure effects have significantly larger amplitudes than those of source 0059+581. Two solid horizontal lines with an absolute value of 60 ps are provided as guides

frequently in the VGOS sessions. Closure delays for triangle ISHIOKA–KOKEE12M–WETTZ13S are shown in the bottom plot of Fig. 6. With replaceable S/X and broadband receivers at the ISHIOKA station and co-located S/X VLBI stations at the sites of both KOKEE12M and WETTZ13S, it is possible to have a similar triangle of stations observing in the S/X mode. Closure delays at X-band from the IVS S/X observations[9] in 2018 and 2019 for triangle ISHIOKA–KOKEE–WETTZELL were calculated and are shown in the top of the figure. Since the source structure effects in VGOS delays are due to the structure at the four frequency bands in the range over 3.0–10.7 GHz in a complex manner and those in the X-band observations are due to structure at the frequencies around 8.4 GHz, the variation patterns in these two plots do not necessarily match with each other. However, the scatters of the closure delays along the variable curves, indicating the random measurement noise level, are far smaller for VGOS observations than for the S/X observations. And even for an extended source like 3C418, those scatters for VGOS observations are at the level of just a few picoseconds. In the bottom plot, the closure delays with absolute magnitudes larger than 150 ps are very likely due to the jumps instead of source structure effects in the delay observables. The delay jump issue is discussed further in the next subsection.

3.3 Delay jumps

In the S/X VLBI mode, multi-band group delay observables have ambiguities, typically with spacings of 50 ns (1 ns = 10^{-9} s) at X-band and 100 ns at S-band, while the VGOS broadband delays have an ambiguity spacing of 31.25 ns; they can usually be resolved based on a priori information prior to performing a geodetic VLBI solution. In the broadband VGOS observations reported here, jumps in group delays have been found to be at least two orders of magnitude smaller than the ambiguity spacing of S/X observations, but only 2–3 times the ambiguity spacing of phase delay at X-band. These delay jumps exist in all of the VGOS sessions.

Closure delays for 3C418 are shown in Fig. 7 for two triangles, GGAO12M–ONSA13NE–WESTFORD and KOKEE12M–WESTFORD–WETTZ13S. For the first triangle, offsets with a magnitude of ∼310 ps occurred during the time period of GMST 22:00 to 05:00 in 13 VGOS sessions. Even more complicated delay jumps appear in triangle KOKEE12M–WESTFORD–WETTZ13S, but no such jumps show up in the two bottom plots of Figs. 4 and 5 for 0059+581 and 0016+731, which cover the same triangle. These delay jumps are more easily identified in a plot of closure delays versus closure TEC as shown in Figs. 9 and 10. They also happen frequently for other extended sources such as 0119+115

[9] https://cddis.nasa.gov/archive/vlbi/ivsdata/vgosdb/.

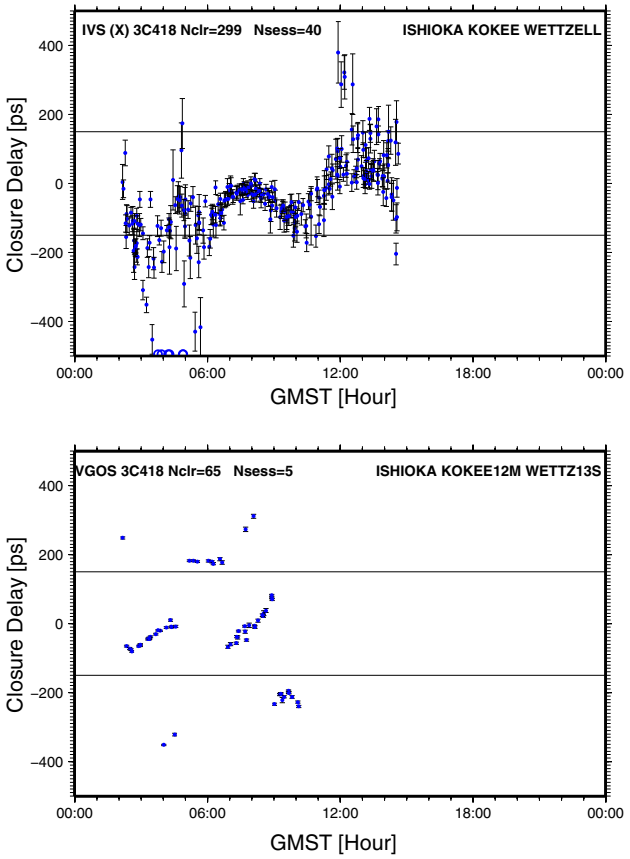

Fig. 6 Plots of closure delays for source 3C418 as a function of GMST for two triangles, ISHIOKA–KOKEE–WETTZELL (top, legacy X-band) and ISHIOKA–KOKEE12M–WETTZ13S (bottom, VGOS). With replaceable S/X and broadband receivers at station ISHIOKA, the first triangle observed in the S/X mode while the second one observed in the broadband mode. These two triangles with a similar geometry allow the direct comparison of structure effects between the legacy VLBI system and the VGOS system. The VGOS triangle observed only in CONT17 and the S/X triangle observed in 40 sessions in 2018 and 2019. The closure delays with absolute magnitudes larger than 150 ps in the VGOS plot are very likely due to delay jumps instead of source structure effects directly, which is discussed in Sect. 3.3. Two solid horizontal lines with an absolute value of 150 ps are provided as guides

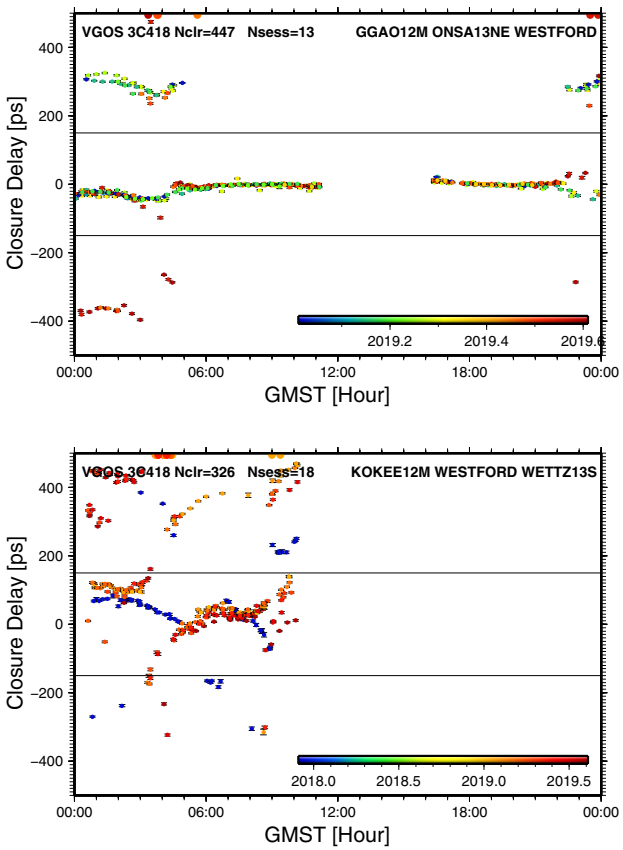

Fig. 7 Closure delays for source 3C418 as a function of GMST for two triangles, GGAO12M–ONSA13NE–WESTFORD (top) and KOKEE12M–WESTFORD–WETTZ13S (bottom). For comparison, closure delays of the second triangle can be seen for sources 0528+483, 0059+581 and 0016+731 in Figs. 3, 4 and 5, respectively

(CARMS=0.39) and 0229+131 (CARMS=0.61). As demonstrated in Figure 3 of Cappallo (2016), which shows the two-dimensional fringe amplitudes as a function of δTEC and group delay, one would expect big jumps in δTEC and in group delay if the wrong peak is mistakenly picked up. Since these jumps tend to happen in the case of extended sources and only a few tens of closure delays and closure δTEC for the CARMS-0.25 sources have jumps, it is likely that the causative factor is source structure. Nevertheless, other reasons are possible as well, for instance, the phasecal problem as found in session VT9007. The sizes of the jumps identified in closure delays seem to be rather stable; however, further studies are necessary to verify if they have a fixed spacing or at what level they can change.

4 Ionospheric effects determined by VGOS

The investigation of δTEC observables in VGOS is interesting because (1) unlike the S/X VLBI system, the design of the VGOS system requires that the dispersion constant in the phase be determined simultaneously with the group delay, and (2) there is a strong correlation, larger than 0.9, between δTEC and group delay estimates based on the current frequency settings, as shown in the variance-covariance analysis of Cappallo (2014, 2016). Observations on the single baseline ISHIOKA–KASHIM34 in Kondo and Takefuji (2016) showed that the standard deviation of the differences between VGOS δTEC observables and the global TEC model was 0.25 TECU. Even though the baseline length of KASHIM34–ISHIOKA (about 50 km) is too short to make a solid conclusion, the differences are far beyond the formal errors of VGOS δTEC observables. The observations of the

Table 4 WRMS δTEC errors determined by closure analysis (in units of TECU)

Session/group (1)	Uniform weighting (2)	Natural weighting (3)
B17337	0.34	0.32
B17338	0.45	0.34
B17339	0.32	0.30
B17340	0.37	0.37
B17341	0.35	0.34
VT9007	0.56	0.73
VT9022	0.33	0.29
VT9035	0.28	0.24
VT9050	0.28	0.26
VT9063	0.32	0.30
VT9077	0.33	0.28
VT9091	0.33	0.32
VT9105	0.32	0.30
VT9119	0.32	0.38
VT9133	0.33	0.27
VT9148	0.33	0.37
VT9162	0.36	0.28
VT9175	0.34	0.24
VT9189	0.39	0.49
VT9203	0.34	0.37
VT9217	0.40	0.32
ALL	0.36	0.35
ALL-19	0.34	0.31
CARMS-0.25	0.15	0.07

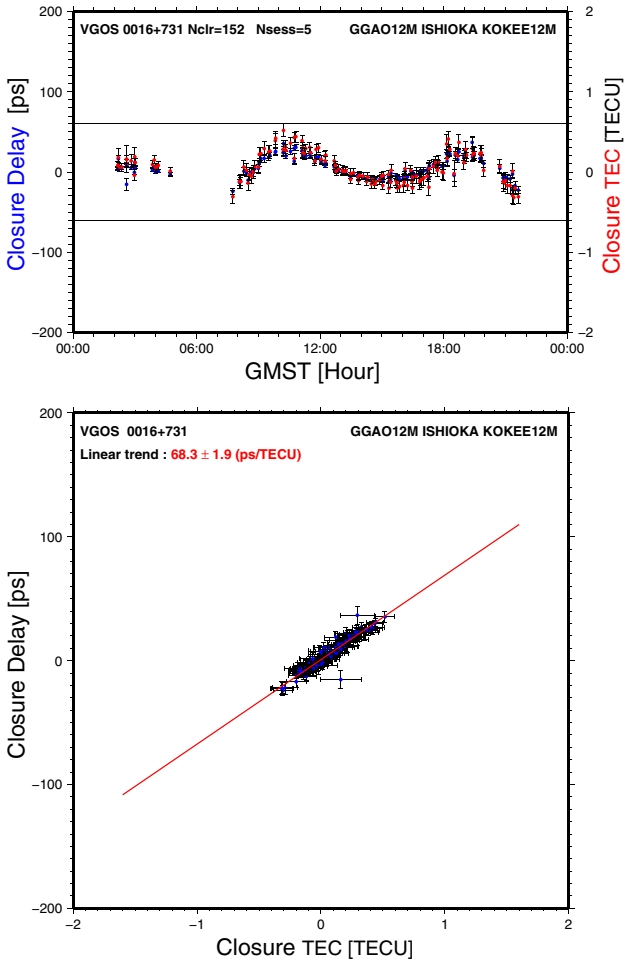

Fig. 8 Demonstration of the strong correlation between δTEC and group delay observables from VGOS. Closure delays (blue dots) and closure TEC (red dots) for source 0016+731 for triangle GGAO12M–ISHIOKA–KOKEE12M as a function of GMST are shown in the top plot, whereas these closure delays versus closure TEC are in the bottom plot. The changing pattern in closure TEC is the same as that of closure delays. There is a strong correlation between them, and the linear trend is 68.3 ± 1.9 ps/TECU

single baseline GGAO12M–WESTFORD in Niell et al. (2018) showed a consistency between the VGOS δTEC observables and differenced GNSS TEC estimates at co-located sites at the level of 1 TECU. A bias of GPS relative to VLBI of -0.5 ± 0.1 TECU was found in the observations on this 600 km baseline. However, neither of these two studies investigated the accuracy of the GNSS-based δTEC used for comparison; consequently, it is not clear if these differences come from the VGOS δTEC estimates or not. The accuracy of, and the potential biases in, VGOS δTEC estimates need to be better understood.

The WRMS δTEC errors are seen in Table 4 to be in the range 0.24 TECU to 0.49 TECU for the 20 sessions excluding VT9007, for which the WRMS error value is 0.73 TECU. Excluding sessions VT9007 and VT9022, the WRMS δTEC errors, labelled as "ALL-19", are 0.31 TECU to 0.34 TECU for the two weighting schemes. They are about one order of magnitude larger than the uncertainties of the δTEC observables, which implies that there are additional error sources in the δTEC observables. The closure analysis of observations of individual sources showed that those additional errors in δTEC are source-dependent. The WRMS δTEC error of the observations for the sources with minimum structure (the CARMS-0.25 group) is only 0.07 TECU based on the natural weighting scheme. Source structure must therefore play a crucial role in the δTEC measurements.

5 Correlation between δTEC and group delay observables from VGOS

A covariance analysis using the VGOS frequency setup predicts a strong correlation between the group delay and δTEC estimates (see Cappallo 2015). It can be more straightforward to understand that correlation and its influence on VGOS observations by analyzing the actual data. Figures 8 and 9

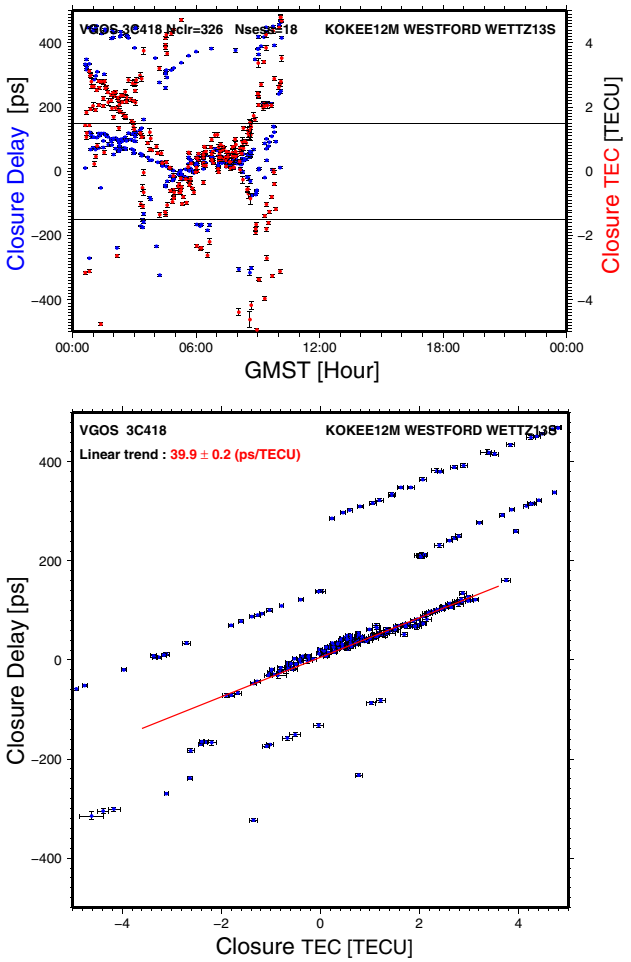

Fig. 9 Demonstration of the strong correlation between δTEC and group delay observables from VGOS and the jumps in them. Closure delays (blue dots) and closure TEC (red dots) for source 3C418 for triangle KOKEE12M–WESTFORD–WETTZ13S as a function of GMST are shown in the top plot, whereas these closure delays versus closure TEC are in the bottom plot. The linear trend between them is 39.9 ± 0.2 ps/TECU. The jumps, which can be two times a certain interval away from the mainstream of points passing the zero closure delay and zero closure TEC, are clearly visible in the bottom plot

demonstrate the correlation by showing closure delays and closure TECs for the sources 0016+731 and 3C418 using two plots each. The trends, obtained from least-square fitting (LSQ), are 68.3 ± 1.9 ps/TECU and 39.9 ± 0.2 ps/TECU for the two sources, respectively.

In the bottom plot of Fig. 9, the points deviating significantly from the red line form basically four straight lines that are parallel to the red line with offsets of 133 ps in delay or 3.3 TECU in δTEC from each other. It confirms the jumps in either or both the group delay and δTEC observables.

Figure 10 shows the closure delays as a function of the closure TEC for all sources and all triangles in the 21 sessions. The closure quantities in the upper plot are from un-flagged observations, whereas those in the bottom plot have at least one of the three observations in a triangle flagged due to the three cases listed in Sect. 2. Two main linear trends between closure delay and δTEC were identified. In the upper plot the data points grouped in the lines parallel to the red line were used jointly to determine the slope with a result of 40.5 ± 0.1 ps/TECU. This estimated value is different from that derived from the closure quantities shown in Fig. 9 for source 3C418 by three times their derived uncertainties, suggesting that the uncertainties from LSQ were too optimistic. Based on the remaining data, another linear trend as indicated by the green line with a slope of 63.8 ps/TECU was determined and found to be in the range of 59.5 ps/TECU to 68.9 ps/TECU depending on the flagging and weighting schemes. The results of these two trends were iteratively determined by excluding the data points larger than five times the WRMS residual. These two linear trends seem to have different origins: (1) the trend in the range 59.9 ps/TECU to 68.9 ps/TECU agrees with the value of $\sim$62 ps/TECU from Cappallo (2016) and is due to the random measurement noise in the channel phases across the four bands; (2) the trend of $\sim$40 ps/TECU results from the systematic variations in the channel phases due to source structure.

Figure 11 is an equivalent plot for CARMS-0.25 sources. Other than the small isolated groups of closures in the upper right and lower left, which are associated primarily with only two of the 28 sources in this category, there are no jumps comparable to those seen in Fig. 10. Were the points for the CARMS-0.25 sources removed, the jumps would still be prevalent. Since the closures shown in Fig. 10 are for all sources, removing the points for the CARMS-0.25 sources would leave the closures for the sources with CARMS greater than 0.25; these are the sources with nominally the more extended source structure. Therefore, our findings indicate that the predominant causative factor of the jumps in delay and δTEC is source structure, which can cause large frequency-dependent phase variations across the four bands. This has been demonstrated by our recent imaging results based on closure phases and closure amplitudes (figures 11 and 12 in Xu et al. 2021a).

6 Conclusions and discussions

We processed the 21 VGOS sessions that have been publicly released and made quality assessments for two kinds of VGOS observables, group delay and δTEC, that are determined simultaneously in the process of broadband bandwidth synthesis. The measurement noise level and the contributions of systematic error sources in these two types of observables were determined by running closure analysis for the whole data set and for the selected sources with minimum structure based on our previous work. By performing closure analysis, two important features in group delay and δTEC observables

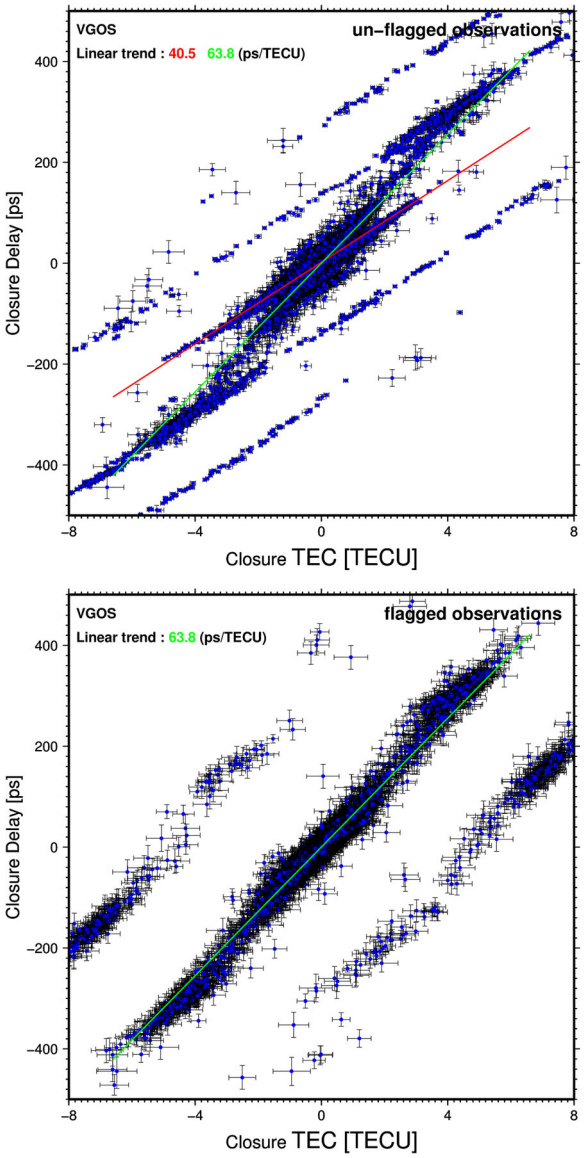

Fig. 10 Closure delays versus closure TEC with un-flagged observations (top) and with at least one of the three observations in a triangle flagged out due to the three cases listed in Sect. 2 (bottom). All sources and all triangles available in the 21 sessions are included. There are two main linear trends between them. The slope of the trend indicated by the red line was determined to be 40.5 ± 0.1 ps/TECU. That of the trend indicated by the green line with a slope of 63.8 ps/TECU was found to be in the range of 59.9 ps/TECU to 68.9 ps/TECU depending on the flagging and weighting scheme, which indicates that it is variable from source to source and from triangle to triangle. In the bottom plot, the vast majority of the closures are from observations of station RAEGYEB in the last four sessions in CONT17; while the closures of the observations flagged due to the other two reasons are nearly all beyond the limits of the plotting axes. The observations of station RAEGYEB have a median SNR of 17-23 in these four sessions, while the rest observations in CONT17 have a median SNR of 92–115. On average, the closures in the bottom plot are from observations with SNRs smaller by a factor of five than those in the upper plot. Another difference in the observations between the two plots is the significant decrease in the channel visibility amplitudes of station RAEGYEB with increasing frequency due to the antenna pointing issue since the second day during the CONT17

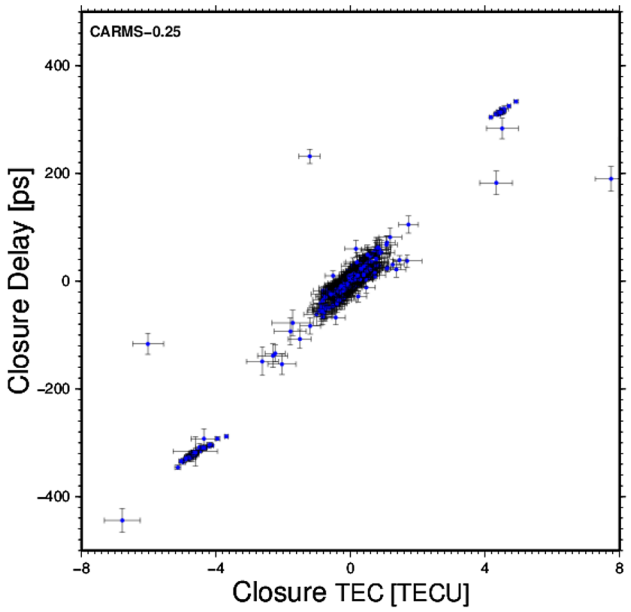

Fig. 11 Equivalent plot to Fig. 10 for the closure quantities of the CARMS-0.25 observations only. Of 20,337 pairs of closure quantities in the plot, there are 17 and 47 pairs in the upper-right and the bottom-left corners, respectively. Most of them involve the observations of sources 0133+476 and 0716+714. The median value of the absolute closure delays in the plot is 2.38 ps, and that of the absolute closure TEC is 0.059 TECU

have been revealed, which are the strong correlation between them and the jumps in both observables.

The random measurement noise level of VGOS group delays was found to be below 2 ps based on the observations from all the VGOS radio sources that have CARMS values smaller than 0.25. The estimated random measurement noise level agrees well with the delay formal errors, as listed in Table 1. However, the contributions from other systematic error sources, mainly source structure related, are at the level of 20 ps, as indicated by the WRMS delay errors for observations of all sources. Due to the significant reduction in measurement noise over the S/X systems, source structure effects with magnitudes of 10 ps are clearly visible. In general, source structure evolves at time scales of a few weeks, which causes the closure delays to change at magnitudes of a few tens of picoseconds. It thus will be a big challenge to correct source structure effects in VGOS in order to fulfill its goals. Evidence for another critical error source in the VGOS system is the presence of discrete jumps in the closure delays and closure TECs, for instance with a delay offset of about 310 ps or integer multiples of that. The likely cause is found to be source-structure-induced phase changes across the four bands (Xu et al. 2021a).

Closure delays on individual triangles were shown for four sources, 0529+483 (CARMS = 0.21), 0059+581 (CARMS = 0.27), 0016+731 (CARMS = 0.31), and 3C418 (CARMS = 0.61) in Figs. 3, 4, 5, and 7 to demonstrate the source structure

effects in VGOS delay observables. By showing the closure delays from the same triangle KOKEE12M–WESTFORD–WETTZ13S in these four figures, the differences in the magnitudes of these effects can be compared among radio sources with structure at various scales as indicated by their CARMS values. The magnitudes of structure effects on the triangle were less than 10 ps for source 0529+483, about 50 ps for source 0059+581, and about 100 ps for source 0016+731; they were larger and more complicated for source 3C418. Delay jumps occurred for the observations of only 3C418 among these four sources.

The random measurement noise level of δTEC observables was determined to be below about 0.07 TECU, which is comparable to the formal errors. The systematic effects are five times larger than that. A strong correlation between group delay and δTEC observables is clearly demonstrated, with two main linear trends. For observations with large structure effects, there is a dominant slope of $\sim$40 ps/TECU. The slope of the second trend is in the range 60 ps/TECU to 70 ps/TECU. Due to this strong correlation and the simultaneous determination of them, group delay and δTEC observables need to be studied together and further. The δTEC estimates from other sources, such as GPS or global TEC models with a sufficient accuracy, might improve the determination of the source structure effects in δTEC observables; based on the stable linear coefficients between delay and δTEC, the source structure effects in group delay observables might be determined without requiring any model of source structure itself. For example, external δTEC estimates can be used to detect the systematic effects in VGOS δTEC estimates, which may be able to predict those effects in delay observables by the linear trends, as discussed in this work.

Delay jumps in the VGOS system need to be understood further. Closure delays have been demonstrated to be useful, and the correlation between group delay and δTEC observables can also be of great help for the delay jump detection. However, the delay spacing of these jumps will have to be studied in detail. The exact origins of the two dominant linear trends between broadband delays and δTEC, the causes of such jumps, and the method to fix them are our near-future work.

Acknowledgements We would like to thank Sergei Bolotin, Arthur Niell, and Brian Corey for their efforts to review the manuscript and for their helpful comments of high quality which improved its comprehensibility. The results reported in this paper were produced using the data owned by the International VLBI Service (IVS) and its international self-funded member organizations. We are grateful to the IVS VGOS stations at GGAO (MIT Haystack Observatory and NASA GSFC, USA), Ishioka (Geospatial Information Authority of Japan), Kokee Park (U.S. Naval Observatory and NASA GSFC, USA), Onsala (Onsala Space Observatory, Chalmers University of Technology, Sweden), Westford (MIT Haystack Observatory), Wettzell (Bundesamt für Kartographie und Geodäsie and Technische Universität München, Germany), and Yebes (Instituto Geográfico Nacional, Spain), to the staff at the MPIfR/BKG correlator center, the VLBA correlator at Socorro, and the MIT Haystack Observatory correlator for performing the correlations and the fringe fitting of the data, and to the IVS Data Centers at BKG (Leipzig, Germany), Observatoire de Paris (France), and NASA CDDIS (Greenbelt, MD, USA) for the central data holds. This research has made use of the Generic Mapping Tools package(https://www.soest.hawaii.edu/gmt/), the pgplot library(https://www.astro.caltech.edu/~tjp/pgplot/), and the SAO/NASA Astrophysics Data System(https://ui.adsabs.harvard.edu/). MHX was supported by the Academy of Finland project No. 315721 and by the National Natural Science Foundation of China (No. 11973023 and 11873077). JMA, RH, SL, and HS were supported by the German Research Foundation grants HE5937/2-2 and SCHU1103/7-2.

Author Contributions MHX and JMA designed the research; MHX performed the research, analyzed the data, and wrote the paper; JMA, RH, SL, HS, and GW contributed to the interpretation of the results and provided suggestions in writing and revising the paper.

Funding Open access funding provided by Aalto University.

Data availability All the VGOS data in the vgosDB data format are available at the CDDIS server: https://cddis.nasa.gov/archive/vlbi/ivsdata/vgosdb/. The closure delays, closure TECs, closure phases and amplitudes from these VGOS sessions are available upon the request to the corresponding author.

References

Altamimi Z, Rebischung P, Métivier L, Collilieux X (2016) ITRF2014: a new release of the international terrestrial reference frame modeling nonlinear station motions. J Geophys Res (Solid Earth) 121(8):6109–6131. https://doi.org/10.1002/2016JB013098

Anderson JM, Xu MH (2018) Source structure and measurement noise are as important as all other residual sources in geodetic VLBI combined. J Geophys Res (Solid Earth) 123(11):10,162–10,190, https://doi.org/10.1029/2018JB015550

Behrend D, Thomas C, Gipson J, Himwich E, Le Bail K (2020) On the organization of CONT17. J Geodesy 94(10):100. https://doi.org/10.1007/s00190-020-01436-x

Bolotin S, Baver K, Bolotina O, Gipson J, Gordon D, Le Bail K, MacMillan D (2019) The source structure effect in broadband observations. In: Haas R, Garcia-Espada S, López Fernández JA (eds) Proceedings of the 24th European VLBI group for geodesy and astrometry working meeting, pp 224–228

Cappallo R (2014) Correlating and fringe-fitting broadband VGOS data. In: International VLBI service for geodesy and astrometry 2014 general meeting proceedings: "VGOS: the new VLBI network, pp 91–96. https://ivscc.gsfc.nasa.gov/publications/gm2014/019_Cappallo.pdf

Cappallo R (2015) Covariance analysis of the simultaneous fit of group delay and dTEC in fourfit. In: Documentation of HOPS, pp 1–5. https://www.haystack.mit.edu/tech/vlbi/hops/simul_ion_fit.pdf

Cappallo R (2016) Delay and phase calibration in VGOS post-processing. In: New horizons with VGOS, pp 61–64. https://ivscc.gsfc.nasa.gov/publications/gm2016/010_cappallo.pdf

Elosegui P, Barrett J, Corey BE, Niell AE, Ruszczyk CA, Titus MA, Bolotin S, Gipson JM, Himwich WE, Neidhart A, Plotz C, de Vicente P, Wakasugi T (2018) An evaluation of VGOS data, precision, and accuracy. AGU Fall Meet Abstr 2018:G33A–05

Fey, AL, Gordon D, Jacobs CS, Ma C, Gaume RA, Arias EF, Bianco G, Boboltz DA, Böckmann S, Bolotin S, Charlot P, Collioud A, Engelhardt G, Gipson J, Gontier AM, Heinkelmann R, Kurdubov S, Lambert S, Lytvyn S, MacMillan DS, Malkin Z, Nothnagel A, Ojha R, Skurikhina E, Sokolova J, Souchay J, Sovers OJ, Tesmer V, Titov O, Wang G, Zharov V, (2015) The second realization of the international celestial reference frame by very long baseline interferometry. Astron J 150(2):58. https://doi.org/10.1088/0004-6256/150/2/58

Kondo T, Takefuji K (2016) An algorithm of wideband bandwidth synthesis for geodetic VLBI. Radio Sci. 51(10):1686–1702. https://doi.org/10.1002/2016RS006070

Niell A, Whitney A, Petrachenko W, Schlüter W, Vandenberg N, Hase H, Koyama Y, Ma C, Schuh H, Tuccari G (2006) VLBI2010: current and future requirements for geodetic VLBI systems. In: IVS working group 3 report, vol 2006, p 28. https://ivscc.gsfc.nasa.gov/publications/ar2005/spcl-vlbi2010.pdf

Niell A, Whitney A, Petrachenko W, Schlüter W, Vandenberg N, Hase H, Koyama Y, Ma C, Schuh H, Tuccari G (2007) VLBI2010: a vision for future geodetic VLBI, p 757. https://link.springer.com/chapter/10.1007/978-3-540-49350-1_108

Niell, A, Barrett J, Burns A, Cappallo R, Corey B, Derome M, Eckert C, Elosegui P, McWhirter R, Poirier M, Rajagopalan G, Rogers A, Ruszczyk C, SooHoo J, Titus M, Whitney A, Behrend D, Bolotin S, Gipson J, Gordon D, Himwich E, Petrachenko B, (2018) Demonstration of a broadband very long baseline interferometer system: a new instrument for high-precision space geodesy. Radio Sci 53(10):1269–1291. https://doi.org/10.1029/2018RS006617

Nothnagel A, Artz T, Behrend D, Malkin Z (2017) International VLBI service for geodesy and astrometry. Delivering high-quality products and embarking on observations of the next generation. J Geodesy 91(7):711–721. https://doi.org/10.1007/s00190-016-0950-5

Petrachenko B, Niell A, Behrend D, Corey B, Boehm J, Charlot P, Collioud A, Gipson J, Haas R, Hobiger T, Koyama Y, MacMillan D, Malkin Z, Nilsson T, Pany A, Tuccari G, Whitney A, Wresnik J (2009) Design aspects of the VLBI2010 system. Progress report of the IVS VLBI2010 committee, June 2009. Tech rep. https://ivscc.gsfc.nasa.gov/publications/misc/TM-2009-214180.pdf

Schuh H, Behrend D (2012) VLBI: a fascinating technique for geodesy and astrometry. J Geodyn 61:68–80. https://doi.org/10.1016/j.jog.2012.07.007

Xu MH, Heinkelmann R, Anderson JM, Mora-Diaz J, Schuh H, Wang GL (2016) The source structure of 0642+449 detected from the CONT14 observations. Astron J 152(5):151. https://doi.org/10.3847/0004-6256/152/5/151. arXiv:1607.04706

Xu MH, Heinkelmann R, Anderson JM, Mora-Diaz J, Karbon M, Schuh H, Wang GL (2017) The impacts of source structure on geodetic parameters demonstrated by the radio source 3C371. J Geodesy 91(7):767–781. https://doi.org/10.1007/s00190-016-0990-x. arXiv:1701.03601

Xu MH, Anderson JM, Heinkelmann R, Lunz S, Schuh H, Wang GL (2019) Structure effects for 3417 celestial reference frame radio sources. Astrophys J Suppl Seri 242(1):5. https://doi.org/10.3847/1538-4365/ab16ea

Xu MH, Savolainen T, Zubko N, Poutanen M, Lunz S, Schuh H, Wang G (2021a) Imaging VGOS observations and investigating source structure effects. J Geophys Res (Solid Earth). https://doi.org/10.1029/2020JB021238

Xu MH, Lunz S, Anderson JM, Savolainen T, Zubko N, Schuh H (2021b) Evidence of the *Gaia*–VLBI position differences being related to radio source structure. arXiv e-prints arXiv:2101.12685. arXiv:2101.12685